Predictability of a Coupled Ocean–Atmosphere Model

B. N. GOSWAMI* AND J. SHUKLA

Center for Ocean–Land–Atmosphere Interactions, Department of Meteorology, University of Maryland, College Park, Maryland

(Manuscript received 19 September 1989, in final form 13 July 1990)

ABSTRACT

The predictability and variability of a coupled ocean–atmosphere model has been investigated by examining the growth of small initial perturbations during the evolution of the coupled system. The ocean model is first integrated in a *forced* mode for a duration of over 24 years beginning with January 1964 in which wind stress forcing for each month is prescribed from the observations. This provides surrogate analysis or *control* run with which predictions from the coupled model can be initiated and compared. Starting from January 1970 with each of the next 181 initial states from the control run, a prediction experiment was carried out for a duration of 36 months each using the fully coupled model. With this large ensemble of prediction experiments, a detailed analysis of growth of initial error and forecast errors was carried out. The SST forecasts are compared with observations as well as the control run. The root-mean-square difference between control and forecasts becomes larger than the standard deviation of the control as well as persistence error in about three months. As a result of differences between the simulated SST in the control run and observations, the forecasts are forced to have initial errors that are comparable to the standard deviation of the observations. Some significant systematic errors in the model are also noted. There is an indication that the forecasts may be improved to some extent by averaging a few of the most recent available forecasts and removing the known systematic error.

Also carried out is a large ensemble of identical twin experiments, each for a duration of 15 years. In one of each pair of experiments a small random perturbation is introduced at the initial time in the surface winds. These experiments have shown that the growth of small initial errors in the coupled model is governed by processes with two well-separated time scales. The fast time scale process introduces errors that have a doubling time of about 5 months, while the slow time scale process introduces errors that have a typical doubling time of about 15 months. The existence of a slow time scale gives us optimism about long-range forecasts of ENSO-type events. However, the fast growth rate tends to saturate at a level that is comparable to the climatological standard deviation. Thus, a key to long-range forecasting of ENSO-type events may lie in the ability to identify those initial states that are not too sensitive to the processes associated with fast growth rate.

The diagnostic analysis shows that the first three empirical orthogonal functions (EOF) of the observed wind stress together explain only about 36% of the total variance. Although the observed wind stress has considerable amplitude in the higher EOFs, it is shown that only the first three components are important for forcing the observed interannual variations using this model. The atmospheric component of the coupled model is not able to simulate these large-scale components of the observed wind stress accurately. This is partly because the atmospheric model is mainly driven by the underlying sea surface temperature anomalies (SSTA) and partly due to the structural differences between the SSTA simulated by the model and the observed SSTA. Thus, a combination of the atmospheric component's tight coupling to the ocean and the ocean model's inability to simulate the SST anomalies correctly seems to be responsible for the rather rapid growth of prediction errors.

1. Introduction

Following the devastating El Niño of 1982–83, several scientists (Cane et al. 1986; Cane and Zebiak 1988; Barnett 1984; Inoue and O'Brien 1984; Barnett et al. 1988; Graham et al. 1987) conducted hindcast–forecast experiments to model past El Niño events. These studies indicate that these events could have been predicted well in advance. While Barnett (1984) and Graham et al. (1987) used purely statistical techniques, Inoue and O'Brien (1984) used an adiabatic ocean model forced by observed surface winds prior to the event. On the other hand, the model used by Cane et al. (1986) was a full, dynamical-coupled model (Zebiak and Cane 1987). The results of these stuides, especially those of Cane et al. (1986), Cane and Zebiak (1988), and Barnett et al. (1988), indicating the possibility of skillful forecasts of these events more than one year in advance, are highly stimulating. The authors noted that the predictions made from the boreal winter were the most successful and those started from spring or early summer were the least successful. The success of a dynamical model in hindcasting the past four events is very encouraging. Unfortunately, there has been only a few

* *Permanent affiliation:* Center for Atmospheric Sciences, Indian Institute of Science, Bangalore-560012, INDIA.

Corresponding author address: Prof. J. Shukla, Center for Ocean–Land–Atmosphere Interactions, 2213 Computer and Space Science Bldg., University of Maryland, College Park, MD 20742-2425.

warm events during the past when reasonable initial condition and verification data could be obtained. The goal of the present study is twofold. First, a large ensemble of predictions is examined to obtain a gross measure of the growth of errors in the (Zebiak and Cane 1987) coupled model. Standard techniques are used for verification, such as calculating root-mean-square error, persistence error, and correlations between the predictions and verifications. This may not be the best approach for El Niño forecasts, but it gives us a gross measure of the coupled model's skill. This part of the study supplements studies done by Cane et al. (1986) and Cane and Zebiak (1988). Second, methodology used in classical predictability studies of the atmosphere is followed to obtain an estimate of the rate of growth of small initial errors in the coupled system.

Classical predictability studies (Lorenz 1963, 1965; Charney et al. 1966; Smagorinsky 1969; and Shukla 1985) have established that the instantaneous state of the atmosphere cannot be predicted beyond a few weeks. However, potential predictability of the low frequency component of atmospheric motion (e.g., monthly and seasonal means) beyond this limit has been demonstrated in recent years (Charney and Shukla 1981; Shukla 1981; Miyakoda et al. 1983; Fennessy et al. 1985). It is argued that the low frequency component is more predictable because it is mainly forced by slowly varying boundary conditions. This concept has received further support from long integrations of general circulation models (GCMs) (Lau 1985; Philander and Lau 1988; Latif et al. 1990). These experiments have shown that low frequency variability in the tropical atmosphere at periods on the order of a year or more is caused not by instabilities of the atmospheric circulation but by variations of the lower boundary condition.

Many simple ocean models such as the linear shallow-water model of the tropical Pacific of Busalacchi and O'Brien (1981), when forced by the observed surface winds, are able to simulate observed sea level changes in the tropical Pacific quite well. This and other simple model studies (Seager et al., 1988; Seager 1989; Bigg and Blundell 1989) and the recent simulation of the tropical ocean circulation by ocean GCMs (Philander and Seigel 1985) during the 1982–83 El Niño demonstrate that low frequency variability in the tropical ocean is caused primarily by the variation in atmospheric forcing and not by instabilities of the mean ocean currents. In contrast, important aspects of middle latitude variability, such as the variability in the Gulf Stream region, are mainly governed by the instabilities of the mean ocean currents.

Although there exist a large number of predictability studies for the atmospheric circulation (as noted earlier), hardly any study of the predictability of the ocean general circulation is found in the literature. In a recent effort, Carton and Shukla (1990) used a multilevel general circulation model of the tropical Atlantic to perform predictability experiments. They found that for the same initial condition, errors in wind stress forcing will produce errors in sea surface temperature (SST) and ocean circulation that grow to their maximum value in about three months. On the other hand, if the same wind stress forcing is applied to quite different initial conditions, the initial errors are found to decay in about three months. However, more experimentation with similar models is required to establish the statistical significance of these results.

An empirical study that attempted to address the predictability of the El Niño–Southern Oscillation (ENSO) in a quantitative manner was performed by Fraedrich (1988). Using annual time series of ENSO indices, he arrived at a doubling time of small errors to be one year. The reliability of this estimate is compromised, however, by the use of annual mean samples and a relatively short time series.

The separate model studies of low frequency variability of the tropical atmosphere and ocean described above give us some hope that the coupled ocean–atmosphere system may have longer range predictability in the tropics. Because the tropical atmosphere and ocean are strongly coupled, the predictability of low frequency variability in the tropics should be addressed using a coupled model. The present study is one such attempt to do so.

The following dynamical elements should be taken into account in developing a conceptual framework for understanding the predictability of the coupled system. We know that the coupled ocean–atmosphere system sustains certain instabilities that arise purely from large scale air–sea interaction. Philander et al. (1984), Yamagata (1985), and Hirst (1986, 1988) have studied these instabilities in detail. Recently Battisti (1988), Battisti and Hirst (1989), and Schopf and Suarez (1988) have proposed that the periodic components of the ENSO phenomenon are merely manifestations of these instabilities. Briefly, this instability mechanism may be described as follows. Consider a modest anomaly in the central equatorial Pacific. The atmospheric response to this SST anomaly produces a burst of westerly surface wind anomalies to the west of the SST anomaly. The oceanic response to the westerly wind anomaly produces a downwelling equatorial Kelvin wave propagating to the east and a upwelling Rossby wave signal propagating slowly to the west. Interacting with the prevailing mean conditions, the downwelling Kelvin wave signal intensifies the SST anomaly, thereby further intensifying the westerly wind anomaly. This positive feedback is the source of the instability. If there were no mechanism to check the growth, the SST anomaly would intensify indefinitely. However, there are at least two mechanisms, one linear and the other nonlinear, that can stop the growth of this instability. The former is a delayed oscillator mechanism related to the equatorial Rossby wave gen-

erated by the westerly wind anomaly in the central Pacific. The upwelling Rossby wave propagates to the west and reflects from the western boundary as an equatorial upwelling Kelvin wave. When this upwelling Kelvin wave reaches the instability region in the central and eastern Pacific it erodes the growth of the SST. The rate of growth of SST due to the Kelvin wave and the travel time of the Rossby–Kelvin waves are important in determining the periodicity of the phenomenon. If there were no other mechanisms affecting the phenomenon, the ENSO would be perfectly periodic and perfectly predictable, as in the models of Battisti (1988) and Andersen and McCreary (1985). Battisti (1988) and Battisti and Hirst (1988) have shown that the nonlinearities associated with oceanic horizontal advection do not have a significant effect on this instability. On the other hand, they showed that the nonlinear effects associated with the upwelling process, too, can check the growth of the instability. These results, which are somewhat model dependent, suggest that the nonlinearities associated with ocean dynamics alone would produce only a regular, predictable oscillation.

This scenario for ENSO events differs in focus from that proposed by Cane et al. (1986), Cane and Zebiak (1987), Zebiak and Cane (1987), and Zebiak (1989). They propose that the changes in the zonal-mean heat content in the equatorial ocean are responsible for the transitions from warm to cold phases and vice versa. According to this hypothesis, the interval between events is the time required by the equatorial heat reservoir to refill. The heat in the ocean is moved around by ocean dynamics. The ocean dynamics, at least in part, involve the wave signals in the equatorial regions. Therefore, the heat content variability could be related to the wave dynamics described above. Thus, the physics of the two scenerios may not be different. However, the mechanism responsible for the aperiodic nature of the refilling is not clear.

The other nonlinearity in the coupled system arises through the coupling process. This is partly because the wind stress forcing of the ocean is a nonlinear function of the wind anomalies and partly because atmospheric heating is also a nonlinear function of anomalies in atmospheric convergence. The predictability of the coupled model depends on how well one component of the model simulates the forcing required for the other component. The coupling processes translate the boundary conditions (SST; surface winds) into these forcings. Being nonlinear, the coupling processes depend sensitively on initial conditions.

Studies of predictability of the atmospheric low frequency variability (Charney and Shukla 1981; Shukla 1981; Shukla 1985) have addressed time scales of a month to a season. On the other hand, the low frequency variability of the tropical ocean, such as the ENSO, has time scales of more than a year. Uncertainties in the atmosphere's behavior enter the ocean through the coupling processes. As the uncertainties in atmospheric low frequency behavior have relatively shorter time scales, the predictability of the coupled system will also depend on the level at which these uncertainties reach a nonlinear equilibrium and how this relatively high frequency *noise* interacts with the low frequency evolution of the ocean circulation.

In the present study the coupled model developed by Zebiak and Cane (1987) is used with the standard set of parameters used by them. Methods used in classical predictability studies of the atmosphere will be employed to derive a quantitative estimate of the predictability of the coupled system. The choice of a model is based on two criteria. First, the coupled model should be able to simulate important aspects of interannual variations in the tropical Pacific realistically. Zebiak and Cane's model satisfies this criterion reasonably well. It is believed that Zebiak and Cane's model, being an anomaly model, avoids certain problems of climate drift associated with coupled GCMs. It is also computationally efficient. Because the model is successful in simulating several features of the observed ENSO variability, it seems to contain the essential nonlinearity and time scale of the system. Because the limits of predictability of a dynamical system mainly depend on the intrinsic nonlinearity and time scale of the system, it is believed that the present results for this particular model will be more generally relevant.

In section 2, a brief description of the model is given, and the results of a control experiment are discussed. Section 3 contains results of a series of forecast experiments and discusses the growth of the forecast errors. The predictability experiments and the growth of small initial errors are discussed in section 4. To get some insight into the dynamics of error growth in the model, a series of diagnostic studies has been carried out. The results of these diagnostic studies are discussed in section 5. Conclusions of the study are presented in section 6.

2. The model and the control experiment

As previously stated, the model by Cane et al. (1986) and Zebiak and Cane (1987, hereafter referred as ZC) is used. The *standard* set of parameters given in ZC is used. This version of the model, including the climatologies required, was provided for this study by the authors. Further insight into the thermodynamics of such a model is provided by Battisti (1988). The strength of the model lies in its ability to simulate some of the important features of the observed ENSO variability, including the irregular recurrence of warm events. Also the asymmetry between the amplitudes of the warm and cold events is realistically reproduced. The weakness of the model is related to the fact that the positive SST anomalies during a mature warm event tend to be too confined meridionally, and the core of the positive anomaly does not move sufficiently

to the west, as it does in the observations. Moreover, the model produces large easterly surface wind anomalies in the eastern Pacific where none are observed during a warm event.

To carry out predictability studies with the coupled model, a dataset representing the true interannual variations of both the atmosphere and ocean is required. Ocean circulation data over a long period of time are not available. Surface wind analyses over the Pacific are, however, available for a relatively long period of time (Barnett 1983; Goldenberg and O'Brien 1981). Therefore, it was chosen to define the interannual variations of the tropical ocean to be given by forcing the ocean model with the observed wind stress anomalies, which are based on subjective analyses of surface winds obtained from ship reports by Goldenberg and O'Brien (1981). A 1–2–1 filter in time, longitude, and latitude was applied to the analyzed winds. To remove an unrealistic trend, the anomalies used are deviations from averages of the same calendar month over the previous four years (Cane et al. 1986; Cane and Zebiak 1987). These analyses were also provided by Cane and Zebiak and consist of monthly mean values for the period January 1964–May 1988. The resolution is 2° × 2°, and the analyzed data extend 29°S–29°N and 126°E–70°W. The control experiment corresponds to a run in which the ocean model is forced by these observed wind stress anomalies. Starting with January 1970, the ocean fields as well as the atmospheric fields produced by the atmospheric model during this run (although they were not used to force the ocean model) are saved once every month. These fields provide the necessary initial conditions for the prediction experiments to be described in section 3.

The physical domain for the ocean model and the locations of regions NINO3 (5°S–5°N and 150°–90°W) and NINO4 (5°S–5°N; 160°E–150°W) are shown in Fig. 1a. The performance of the ocean model in simulating the interannual variations is shown in Fig. 1b, where the NINO3 averaged SST anomalies (SSTA) simulated by the forced model is compared with observations from the Climate Analysis Center (CAC). The model simulates warm events reasonably well. However, the correlation between the observed and simulated SSTA is poor during intermediate periods. The rms error between the observed and simulated SST is 0.72°C. This is comparable to the standard deviation (=0.71°C) of the simulated time series, but is smaller than the standard deviation (=0.92°C) of the observed sea surface temperature anomaly over NINO3 region (NINO3 SSTA). This discrepancy between the model simulation and the observations may be partly due to the inadequacy of the ocean model and partly due to the errors in the analysis of wind stress used as observations.

A modified version of the model, including a more complete flux parameterization, was used by Seager (1989) to simulate the total SST variations in the Pacific. The performance of the model and its deficiencies are discussed in detail in that study.

Next results from a series of prediction experiments are presented. Because an adequate data assimilation system and analysis scheme for the coupled system is not currently available, the initial conditions for the prediction experiments will be derived from the control experiment as in Cane et al. (1986). However, the verification strategy for these predictions is not obvious. Forecast errors for SST anomalies shall be presented, as this is the only oceanic field for which reasonable observations are available. Also compared are the predictions with the control simulation because one can verify all the coupled model variables in that case. However, the difference between the coupled model simulation and the control is not strictly the forecast error. In any case, section 3 shows that this comparison provides insight towards understanding how small errors grow in the coupled model.

3. The prediction experiments

Each prediction experiment is started with an initial condition saved once every month during the control experiment starting with January 1970. The coupled model then determines the future evolution for a duration of 36 months. This means that the initial conditions for the ocean are model simulations forced by the observed wind stresses, but during the prediction period the coupled model evolves as an interacting-coupled system. In this manner, 181 forecast experiments were carried out for 181 initial conditions corresponding to each month during the period January 1970–January 1985.

a. Comparison between control and coupled model predictions

In this subsection, the manner in which the differences between the control run forced by observed surface winds and the coupled run grow with time is examined. The differences between the control and prediction experiments are not, strictly speaking, forecast errors—they merely represent the differences between the uncoupled run with observed wind stress forcing and the coupled model predictions, both starting from the same initial conditions. It is worth noting that the control simulation may contain some systematic error (or deficiencies) of the ocean model. Therefore, a part of the systematic error in the coupled model originating from the ocean component is subtracted out when differences between the control and the coupled predictions are calculated. This will give some idea about how the wind stress produced by the coupled model begins to depart from observations, which are analyses based mainly on ship reports.

To illustrate the evolution of these predictions, NINO3 SSTA from the coupled model are shown in Fig. 2. It shows a variety of dependence of the predic-

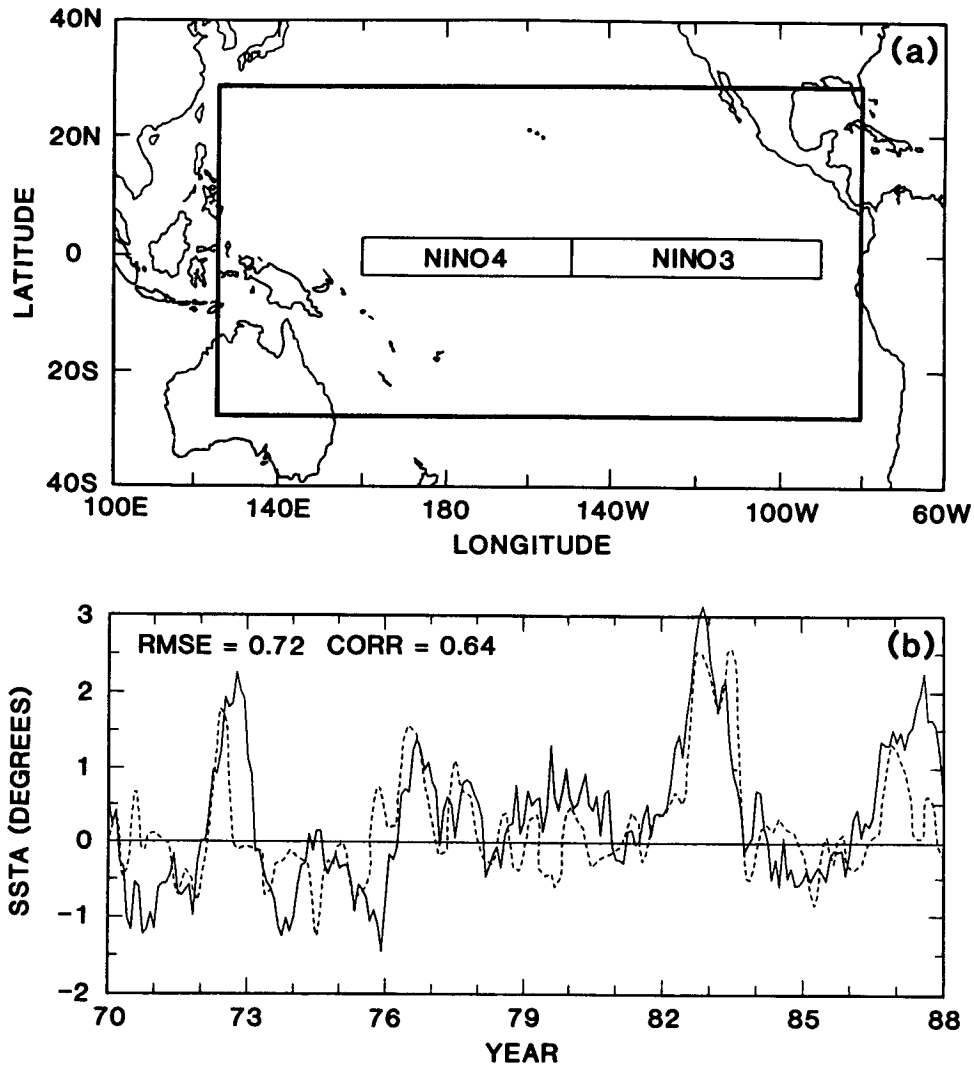

FIG. 1. (a) The geographical domain for the ocean model and the two regions NINO3 and NINO4. (b) NINO3 averaged SSTA in the control experiment (dashed curve) versus the observed (solid curve) over the same region. The rms error and correlation between the two series are shown.

tions on the initial conditions. The model appears to be successful in capturing the growth phase of some of the major El Niño events; however, for many cases a large warm event is predicted even when there is no warm event in the control. To further illustrate the variety of evolution of the predictions, six pairs of subjectively selected predictions are shown in Fig. 3, each pair starting from two consecutive months. Figures 3a,b show that the two predictions in each pair not only follow each other during their evolution but also follow the control closely throughout most of the 36 months. Figures 3c,d show that the two predictions in each pair follow nearly identical evolutions but diverge significantly from the control after about 12 months. On the other hand, Figs. 3e,f show that the two predictions in each pair start diverging rapidly from each other within a couple of months.

The differences between the control and corresponding one-month, three-month, and six-month predictions of NINO3 SSTA for all the initial conditions are shown in Fig. 4. An examination of these predictions and the corresponding prediction differences shows that the one-month differences (Fig. 4a) remain small for all the initial conditions. However, the three-month differences (Fig. 4b) tend to become quite large for some initial conditions. The standard deviation (SD) of the three-month differences becomes comparable to the SD of the control NINO3 SSTA. By six months (Fig. 4c), the differences have become so large that their SD becomes larger than the SD of the control NINO3 SSTA. This means that two six-month predictions made from slightly different initial conditions diverge as much as two randomly selected states of the control. Note that the largest differences

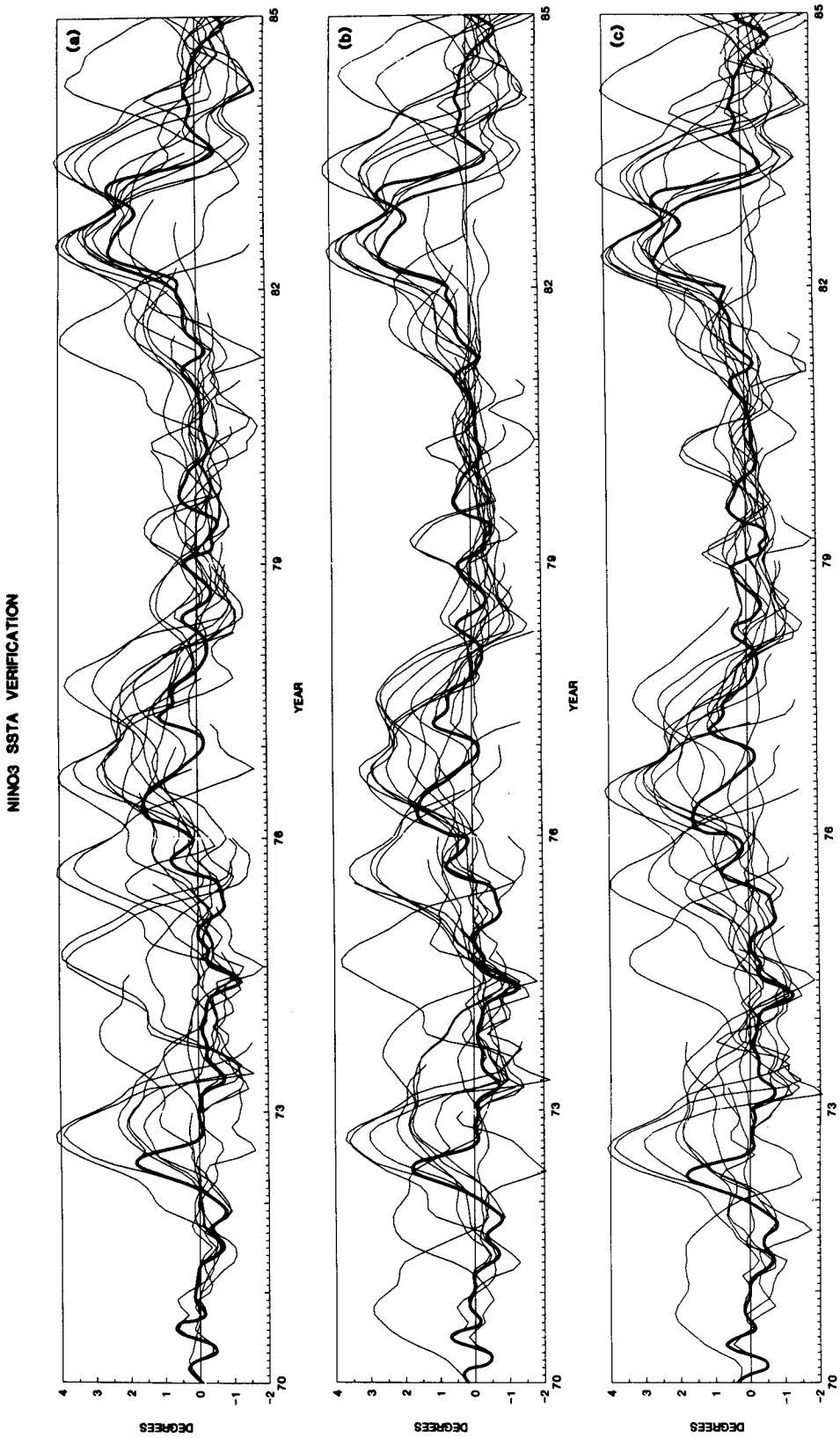

FIG. 2. The complete ensemble of predictions for NINO3 SSTA. The heavy curve represents the control, while the light curves are the predictions. Each panel contains one-third of the total predictions for clarity. (a) All predictions made from January, April, July, and October. (b) All predictions made from February, May, August, and November. (c) All predictions made from March, June, September, and December.

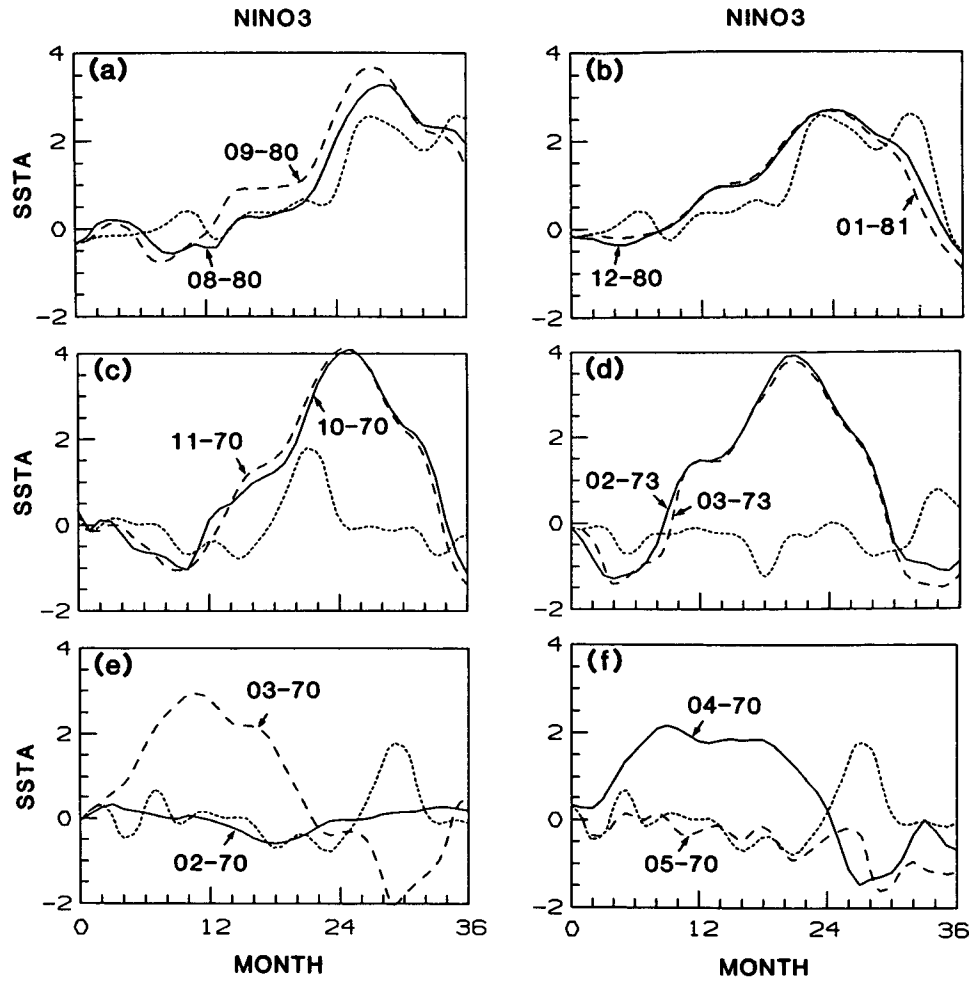

FIG. 3. Verification of six pairs of subjectively selected predictions of NINO3 SSTA starting from two consecutive months. The dotted curve is the control in each panel, and the solid and the dashed curves are two predictions starting from two consecutive months. The starting months are shown as: month-year.

occur for comparisons corresponding to the months after a warm event. In other words, the largest differences occur for the initial conditions corresponding to the peak and decaying months of the warm events. This is a systematic error of the coupled model. As a result, the average of the predicted SSTA in Fig. 4 is always larger than the average of the control SSTA. The question of systematic errors will be discussed later in this section.

Let us denote the prediction for any dynamical variable made from the ith initial condition ($i = 0, 1, \cdots, 180$; $i = 0$ corresponding to January 1970) and for the jth month ($j = 0, 1, \cdots, 36$; $j = 0$ corresponds to the initial condition itself, which is the control run) as ψ_{ij}. Let an averaged prediction minus control ($P - C$) error (E) for the jth month of prediction be defined as

$$(P - C)E_j = \left[\frac{1}{181}\sum_{i=0}^{180}(\psi_{ij} - \psi_{i+j,o})^2\right]^{1/2}. \quad (1)$$

Similarly, a persistence error for the jth month of prediction is defined as

$$(PE)_j = \left[\frac{1}{181}\sum_{i=0}^{180}(\psi_{ij} - \psi_{i,o})^2\right]^{1/2}. \quad (2)$$

The prediction minus control errors averaged over all 181 predictions and the persistence errors averaged for all 181 initial conditions for NINO3 SSTA are shown in Fig. 5a. It also shows the standard deviation of the control NINO3 SSTA. It should be noted that the predictions are better than persistence only for the first three months. Also, the errors become larger than the natural variability (i.e., the standard deviation) after three months. The errors tend to saturate by about nine months. As an alternative measure of the success of the predictions, the correlations between the predictions and the verifications from the control are shown in Fig. 5b. It is seen that the correlation decreases rapidly to a value of about 0.55 by four months and

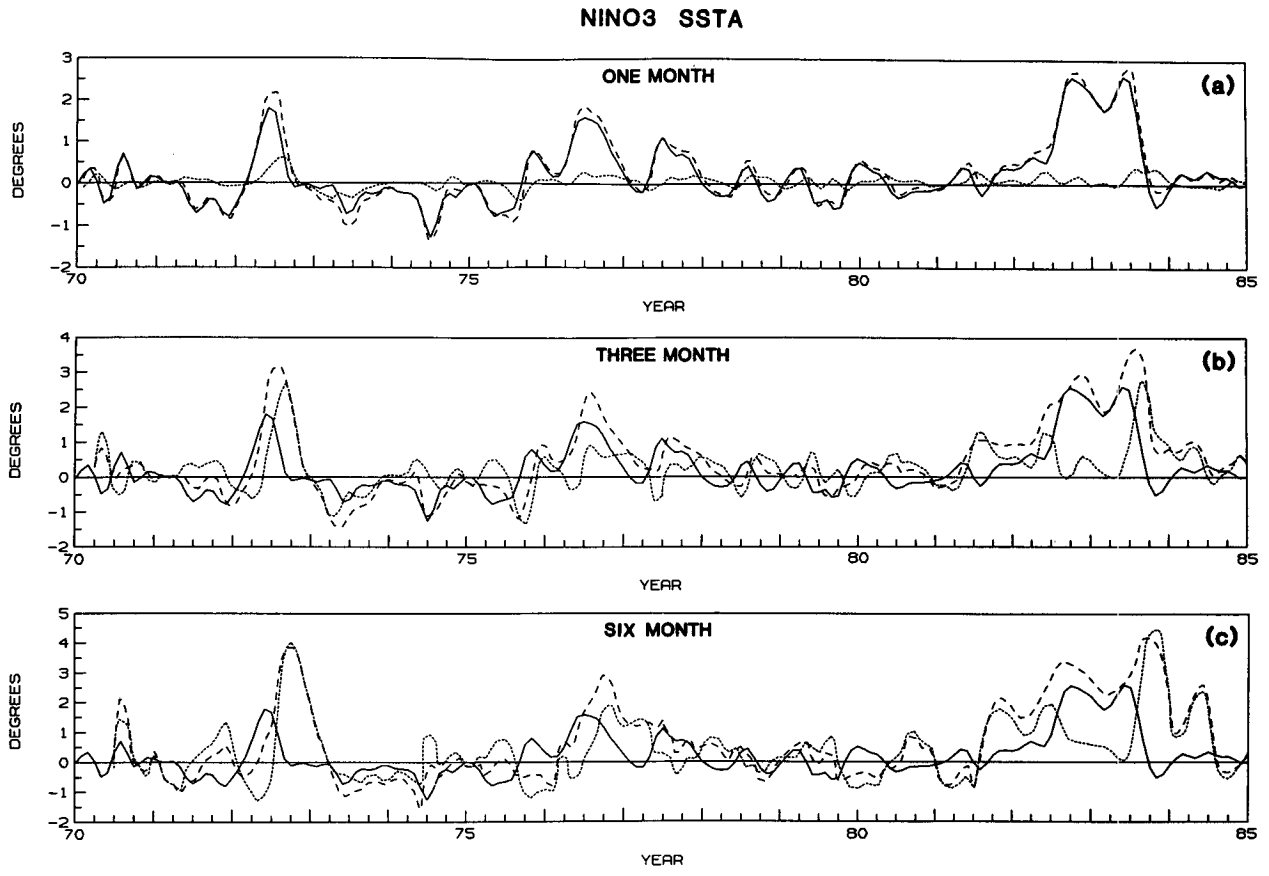

FIG. 4. Comparison of predictions of NINO3 SSTA with control for all (a) one-month predictions, (b) three-month predictions, and (c) six-month predictions. Solid curve = control, Dashed curve = predictions, Dotted curve = error (predictions minus control).

remains somewhat steady until about 12 months. Beyond 12 months, the correlation further decreases.

It was noted earlier that the model predictions show a systematic error, which can be defined as the average prediction error (mean of all the predictions minus mean of all the verifications from the control run). The systematic error of the model is shown in Fig. 6a by the solid curve. Largest positive bias occurs for a lag of about 12 months. Whether the prediction skill could be improved by removing this systematic error from the predictions was examined. The errors calculated after subtracting the systematic error from the predictions is shown in Fig. 6a by the dotted curve. It is seen that the skill of the predictions beyond three months improves to some extent by this procedure. However, the errors remain larger than persistence beyond three months. The possibility of improving the skill using a *lagged averaged forecast* method (Hoffman and Kalnay 1983) is explored in Fig. 6b. It shows that if the systematic error is removed and the six predictions initiated from the last six months are averaged, the predictions improve significantly beyond six months; however, the error is still higher than the long-term standard deviation of the control.

So far, error statistics have been discussed by examining the SSTA over only the NINO3 area. To examine the character of the growth of errors outside this region, the RMS errors as measured by the difference between the control and the predictions averaged over the whole ocean domain were also calculated. In addition to the SSTA, the growth of prediction minus control errors were calculated for three other fields (thermocline height anomaly, H, and the zonal (u_a) and meridional (v_a) component of the surface winds). Results of these calculations (not shown) indicate that the character of the error growth, particularly for the SSTA, remains the same. For the other variables also, the errors tend to reach a plateau by about nine months.

Some studies (Battisti et al. 1989; Zebiak and Cane 1987) have indicated that there may be some seasonality in the growth of errors in the coupled system. Figure 7 examines the dependence of the prediction minus control errors of NINO3 SSTA on the initial conditions corresponding to different months of the year. In agreement with the results of Zebiak and Cane (1987), some signature of extended forecast skill is evident for forecasts starting with initial conditions corresponding to September through February. These re-

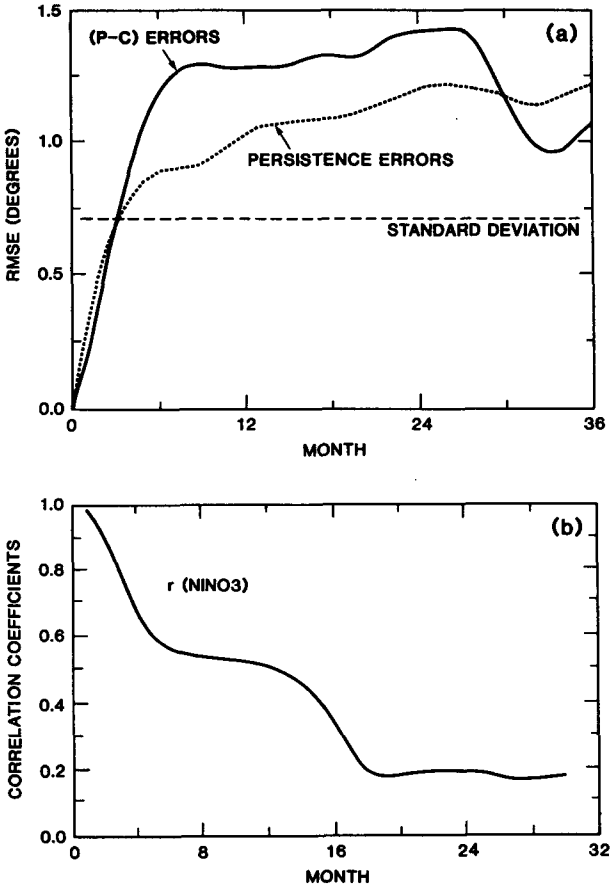

FIG. 5. (a) Rms prediction minus control ($P - C$) error of NINO3 SSTA using all 181 predictions (solid). The persistence error (dotted) and standard deviation (dashed) of the control NINO3 SSTA are also shown. (b) The correlation coefficients (r) between the predictions and verifications of NINO3 SSTA from the control.

sults are consistent with Battisti (1989b), who argues that the seasonal changes of the stability of the coupled system may result in a seasonality in prediction skill. However, it should be noted that each rms error in Fig. 7 comes from an ensemble of only 15 predictions.

b. NINO3 SSTA forecast errors

In this subsection, the SSTA forecasts averaged over the NINO3 area are compared to observations. The observed SSTA is taken from the analysis of surface marine temperatures described by Reynolds (1988). Forecast error is defined in a manner similar to Eq. (1) where the verifications, $\psi_{i+j,o}$, are now replaced by the corresponding observations. The root-mean-square forecast error derived from all 181 forecasts for NINO3 SSTA is shown in Fig 8. Note that there are large errors in the initial condition itself. This is consistent with Fig. 1b and is partly due to inaccuracies in the observed wind stress and partly due to the deficiencies of the ocean model in correctly simulating the SSTA. The errors for NINO3 SSTA tend to become larger than the standard deviation of the observed NINO3 SSTA by about four months. The forecast errors remain larger than the persistence error for nearly the entire period of forecasts. However, the forecast errors became smaller than persistence at leads between 9 and 18 months if the systematic error is removed from the forecasts.

4. Predictability studies

In this section, methods used in classical predictability studies of the atmosphere are adopted to determine the time scale of growth of small initial errors. The control run is used to define the initial conditions for coupled model runs. Following Lorenz (1982) the growth of error between two coupled model runs for which initial conditions were only one month apart in the control run were calculated. These calculations were repeated for initial conditions being 2, 3, 4, · · · 12

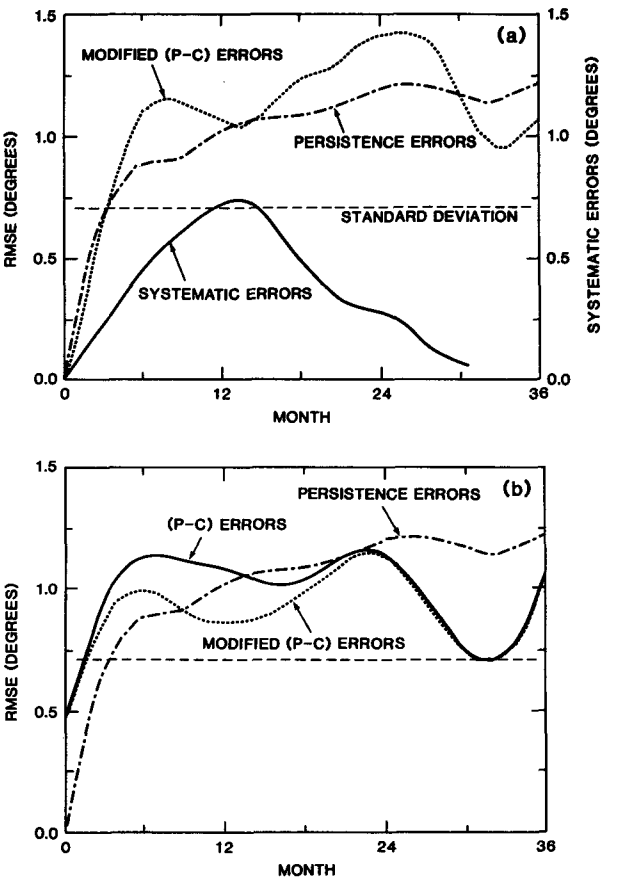

FIG. 6. (a) The systematic error of NINO3 SSTA predictions as defined by mean of all predictions minus mean of all verifications (solid). The modified ($P - C$) errors (dotted) after removing the systematic error compared with the persistence (dot–dash) and the standard deviation of the control (dashed). (b) The solid curve is the lagged averaged errors, from predictions constructed by averaging the six predictions starting from the last six months. The lagged averaged errors after removing the systematic errors (dotted), and the standard deviation (dashed), are also shown.

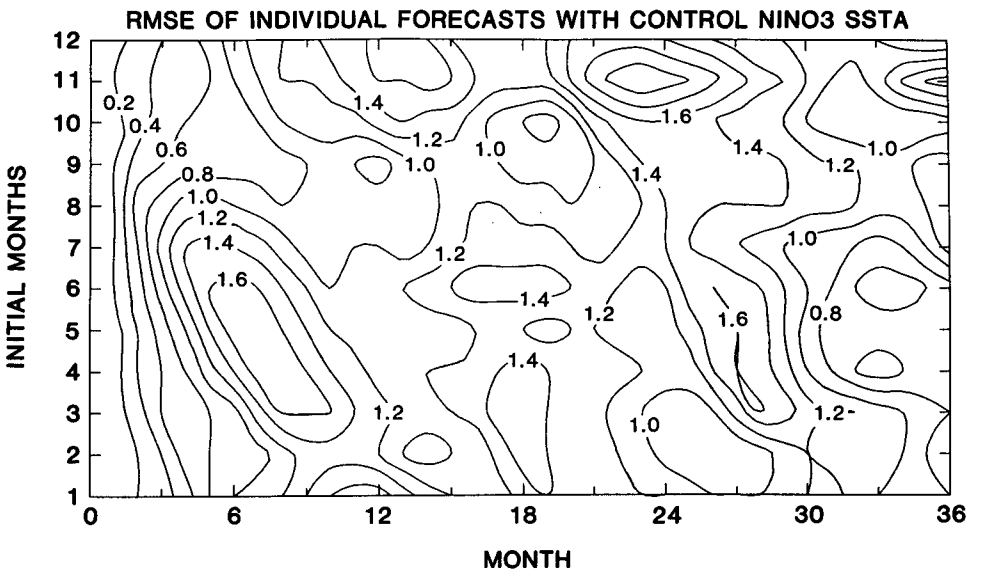

FIG. 7. Dependence of rms ($P - C$) error of individual forecasts on the initial conditions corresponding to different months of the year (1–12 refer to January–December, respectively). Contour interval is 0.2°C.

months apart in the control run. We also conduct a series of *identical twin* experiments with the coupled model by introducing small random initial perturbations.

The rms growth of initial error corresponding to the kth month prediction (defined by the difference between the control and predictions) at the prediction month $j + k$ is given by

$$E_{k,j+k} = \left[\sum_{i=0}^{180-k} (\psi_{i,j+k} - \psi_{i+k,j})^2/(181 - k) \right]^{1/2} \quad (3)$$

with $j = 0, 1, \cdots, 36 - k$ and $k = 0, 1, \cdots, 36$.

These quantities calculated from the forecast data up to a maximum of $k = 12$ are shown in Fig. 9. The first curve labeled E_1 represents the mean growth of error for all the cases for which the initial error was equal to the one-month prediction error compared to control. Similarly, the second curve, E_2, represents the mean growth of error for all cases with initial error equal to the two-month prediction error compared to control, and so on. Note that for the first few curves (representing growth of small initial errors), the error grows rather rapidly during the first month and then grows at a much slower rate. It is likely that the rapid

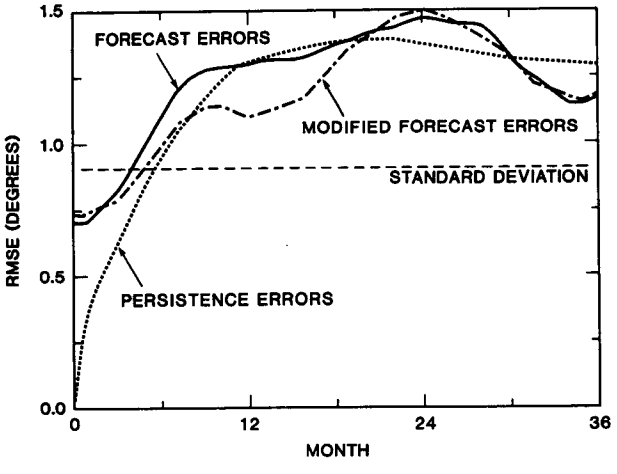

FIG. 8. NINO3 SSTA forecast errors as compared to observations (solid). The persistence error (dotted) and the standard deviation of observed NINO3 SSTA (dashed) are also shown for comparison.

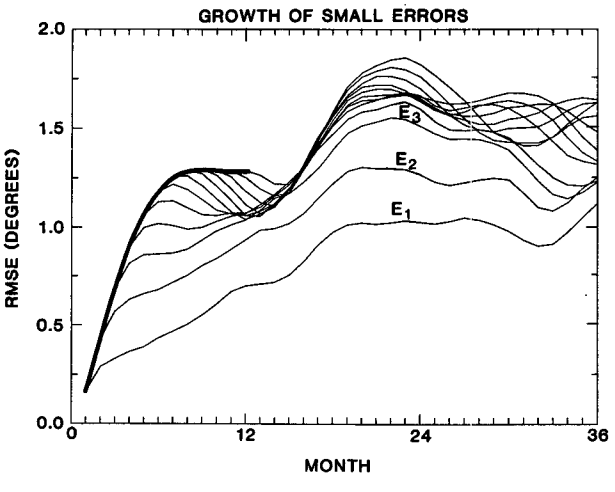

FIG. 9. Growth of small errors for NINO3 SSTA calculated from the 181 available predictions. The lowest light curve shows the growth of mean one-month ($P - C$) errors. The next higher light curve shows the growth of mean two-month ($P - C$) errors and so on. The heavy envelope corresponds to the error curve in Fig. 5a.

increase of error during the first month is a result of the uncertainties introduced by the atmospheric processes having shorter time scales and faster growth rates. The slower growth rate during the following months could be mainly due to the slow coupled process. Also note that large initial errors tend to evolve in a significantly different way. In fact, large initial errors corresponding to six-month or more prediction errors compared to control tend to decrease initially and later increase rapidly. Recall from Fig. 5a that for predictions beyond three months, the errors are already comparable to the natural variability of the system. When such large initial errors are introduced into the coupled system, the system tends to go through an adjustment process.

To get a quantitative estimate of the growth rate of small initial errors, one assumes that the equation governing the growth of error is given by (Dalchar and Kalnay 1987):

$$dE/dt = (\alpha E + S)(1 - E/E_\infty) \qquad (4)$$

where α is the growth rate, S is the amount of error introduced by model deficiencies, and E_∞ is the saturation value of the error. Equation (4), is a modified version of the error growth equation used by Lorenz (1982). The solution of Eq. (4) was fit to the growth of one-month prediction errors (E_1 of Fig. 9). This is shown in Fig. 10a. It gives a growth rate of $\alpha = 0.15$ $(\text{month})^{-1}$ or a doubling time of about 4.5 months.

Any initial error, small or large, would finally saturate at a value corresponding to the model's natural variability (given by the model's standard deviation). The standard deviation of the model's NINO3 SSTA (obtained from a relatively long coupled run) is about 1.5°C. It is clear from Fig. 9 that although the one-month prediction error seems to have reached a plateau, it obviously has not reached its final saturation value during the three-year predictions. Thus, the growth rate obtained from Fig. 10a may not represent the whole story. The fact that the one-month prediction errors remain in a plateau for nearly 1½ year indicates that there may be other processes with different time scales that are responsible for the larger natural variability of the system.

To test this speculation and to obtain a more reliable estimate of the growth rate, a series of identical twin experiments of sufficiently long duration was carried out. First, 151 *control forecast* experiments were conducted, each for a duration of 15 years (180 months). The 151 different initial conditions for these forecast experiments were derived from the control experiment. The range of predictions in these experiments was extended as it is anticipated that the small errors introduced in them will take longer to reach saturation. Next, 151 *perturbed forecast* experiments were conducted. The perturbed forecast experiments were identical to the control forecasts except for a small random perturbation introduced at the initial time on the zonal

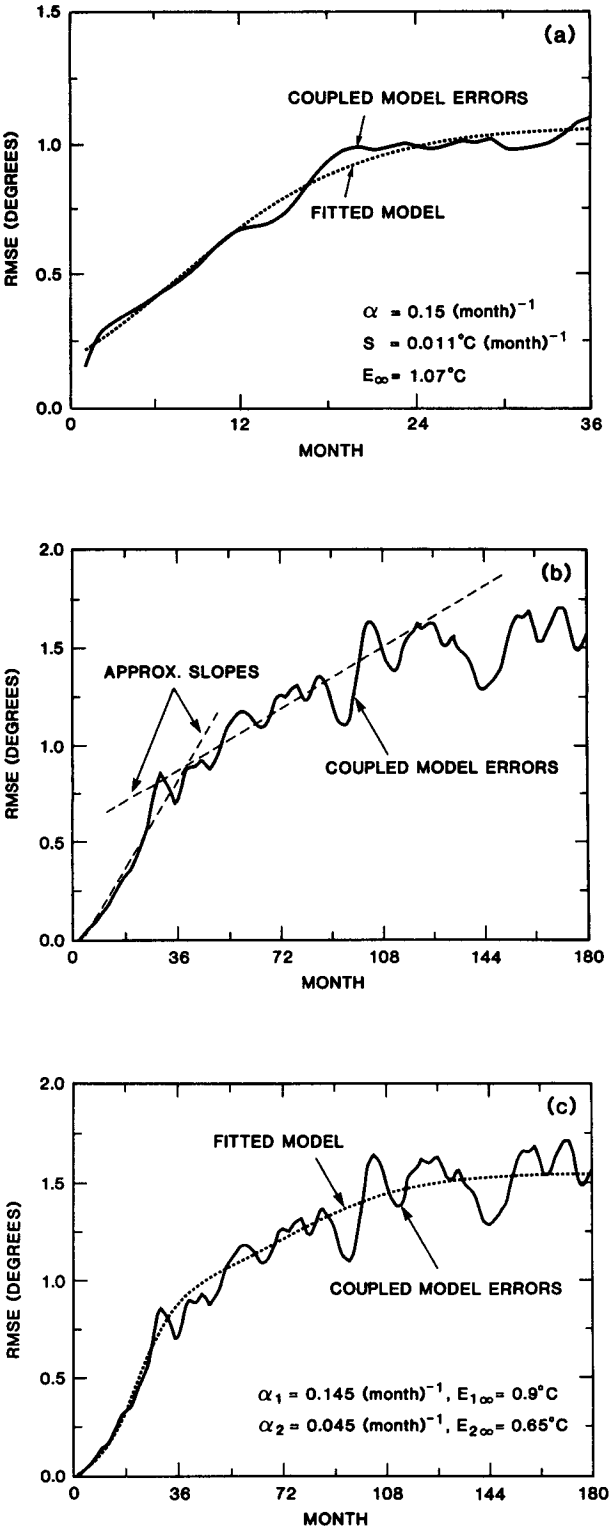

FIG. 10. Empirical model for the growth of small errors. (a) Growth of one-month ($P - C$) errors (solid) and the fitted model (dotted). (b) Same as (a) but rms error from 151 identical twin experiments due to small random initial perturbation on the surface winds. The dashed curves show approximately the two different slopes of the curve. (c) The fitted model for the error curve in (b).

(u_a) and meridional (v_a) components of the surface winds. The random perturbations have a Gaussian distribution with zero mean and standard deviation of 0.2 and 0.1 m s^{-1} for perturbations on u_a and v_a, respectively. The growth of errors averaged over the 151 cases is shown in Fig. 10b. The initial errors in SSTA in this case are identically zero, but the small initial errors in the surface winds introduce small errors in the SSTA within one month that subsequently grow. As expected, the smaller initial errors take longer to reach saturation.

Two points are worth noting in Fig. 10b. First, the error fluctuates around 1.5°C for the last five years. Thus, it is assumed that the error has reached its saturation value. Second, note that the error growth curve has two slopes, approximately shown by the dashed lines in Fig. 10b. This indicates that the growth of errors in the coupled model is governed by two processes with two quite different time scales. One of the processes has a faster growth rate and tends to saturate at around 1°C, and the other has a much slower growth rate. To obtain some quantitative estimate of the growth rates, it is assumed that the error growth can be approximated by a linear combination of two processes, each governed by a different exponential growth rate. Thus,

$$E(t) = E_1(t) + E_2(t), \tag{5}$$

where

$$dE_1/dt = (\alpha_1 E_1 + S_1)(1 - E_1/E_{1\infty}), \tag{6}$$

and

$$dE_2/dt = (\alpha_2 E_2 + S_2)(1 - E_2/E_{2\infty}). \tag{7}$$

As discussed before, α_1 and α_2 represent the two growth rates, and the total saturation value is given by $E_\infty = E_{1\infty} + E_{2\infty}$. Similarly, S_1 and S_2 represent two source terms arising due to the inadequacies of the model. Equation (5) is fitted to the error growth curve shown in Fig. 10b, for which $E_\infty = 1.55$. The best fit is obtained for $E_{1\infty} = 0.9$°C. The fast growth rate is found to be $\alpha_1 = 0.145\ (\text{month})^{-1}$, corresponding to a doubling time of 4.8 months. The slow growth rate is found to be $\alpha_2 = 0.045\ (\text{month})^{-1}$, corresponding to a doubling time of 15.3 months. The empirical model obtained this way is shown in Fig. 10c. The success of the model with the two time scales is rather striking. It is interesting to note that the fast growth rate obtained from the identical twin experiments is very close to the one obtained from Fig. 10a by fitting the growth of one-month prediction errors. This is because, within three years, the slow process does not affect the error growth appreciably. The existence of two growth rates is also seen in the growth of errors in other variables of the model such as u_a, v_a, NINO4 SSTA, etc.

It is worth noting that the two time scales associated with the error growth in the coupled model are somewhat analogous to the different growth rates of errors for high-frequency synoptic disturbances and low-frequency planetary waves in the atmosphere. The important difference seems to be that the two time scales associated with the error growth in the coupled model are well separated.

It is interesting to note that the time scale for the fast growing process is very close to that of the coupled instability discussed by Philander et al. (1984), Yamagata (1985), and Hirst (1986, 1988). As discussed by Battisti (1988), the dominant ENSO-type variability in the ZC model is a result of such a coupled instability and its interaction with the wave dynamics of the equatorial Pacific. In particular Battisti (1988) noted that the coupled instability in the ZC model is dynamically similar to the instability in model IV of Hirst (1986). It is noted that the *e*-folding time for the fast error growth ($1/0.145 \sim 6.9$ months) in the ZC model (Fig. 10c) corresponds closely to the *e*-folding time of about 200 days for the growing mode of Hirst's model IV. Even though one needs to take into account the difference between certain parameters in the ZC model and Hirst's model IV, the correspondence between the two growth rates is remarkable. This strongly suggests that the coupled instability in the system could be responsible for the fast growing part of the error growth.

The slower growth rate can also be related to the physics of the ZC model as discussed by Battisti (1988, 1989b) and Battisti and Hirst (1989). The wave reflection, together with the local instability process, sets a time scale for the model ENSO cycle that is not perturbed by the presence of a small amount of high frequency noise (Battisti 1988). The low frequency behavior in the model is dominated by the ENSO cycle that has a half-period of about two years; this is the time interval between largest accelerations in the system, i.e., the time interval when the system is expected to be shooting through the unstable equilibrium. Therefore, one expects the growth rate associated with this low frequency mode to have an *e*-folding time between a quarter-cycle ($\sim$12 months) and a half-cycle ($\sim$24 months). Thus, the growth rate for the slow evolution of errors ($1/0.045 \sim 22$ months, Fig. 10c) seems to be associated with the ENSO-type low-frequency variability in the model. The model physics dictates the following zero order classification scheme for predictability of initial states for the low-frequency ENSO mode. The basic states prescribed in the coupled model corresponding to January and February are stable (Battisti 1988); thus one could expect longer predictability of initial states corresponding to these results. This is consistent with the results of the prediction experiments (Fig. 7), as well as with the hindcast study of ENSO events by Cane et al. (1986). The predictability seems to be minimum for initial states corresponding to Northern Hemispheric spring and summer. This may be partly due to the fact that the basic states start becoming more and more unstable beginning with the month of April (Battisti 1988). Moreover, the coupling in the model introduces high frequency noice in the system mostly during boreal spring.

The existence of a high level of high frequency noise also makes the system less predictable. Similar arguments about the dependence of the predictability of the low frequency mode on the seasonal cycle were made earlier by Battisti (1989b).

The existence of a slow time scale in the coupled system had been intuitively suggested by Cane and Zebiak (1988) and has been the basis for their optimism for the prediction of ENSO events at long lead times. These results suggest that indeed there is a basis for optimism for long-range predictability of ENSO events. However, this success will depend on our ability to select those initial conditions that are insensitive to the fast growing instabilities. This conclusion is supported by the experience of Cane et al. (1986) with their hindcast experiments that show that forecasts made from Northern Hemispheric winter are most successful in predicting ENSO while those made from boreal spring are the least successful. As shown by Battisti and Hirst (1989), the background mean conditions are least unstable to the coupled instability during Northern Hemispheric winter and most unstable during summer.

5. Diagnostic analysis of the error growth

In section 3, it was shown that the RMS difference between the control and the predictions of the coupled model becomes larger than the climatological standard deviation of the control after three months. This time is longer than the limit on the deterministic predictability of the atmospheric motions but much shorter than the time scales associated with low frequency oceanic variability such as the ENSO. It is also noted from Fig. 5a that the errors during the first three months of predictions are comparable to persistence errors. The fact that the predictions of the coupled model become worse than the persistence forecasts for the SSTA after three months indicates that the coupled model introduces errors early during the prediction period that grow to be sufficiently large by three months. In this section, results from a series of diagnostic studies aimed at understanding the source of errors in the coupled model predictions are presented.

The control run was obtained by forcing the ocean model with the observed surface winds; therefore, in order that the coupled model produce skillful predictions, the atmospheric component of the model should be able to produce surface winds compatible with the observations. Hence, the coupled model predictions for the zonal component of the surface wind stress (τ^x) were compared with observations averaged over NINO4. The NINO4 area is chosen for this purpose because the largest wind stresses occur over this region. This comparison is shown in Fig. 11. It shows that within one month the amplitude of the prediction errors for τ^x becomes as large as that of the observed τ^x. This is further illustrated in Fig. 12, where the growth of errors of NINO4 τ^x averaged over all 181 predictions is presented. This also shows that the experiment starts with a one-month prediction error that is larger than the natural variability of the observed τ^x. During subsequent months, the prediction error for τ^x grows slowly. Therefore, it appears that the inability of the atmospheric model to produce reasonable surface winds is a major source of error in these predictions.

Having identified the wind stress as an important source of errors in the coupled model, the structure of the surface winds produced by the atmospheric model are further studied and compared with the observations. This is done by a series of empirical orthogonal function (EOF) analyses of the various fields. The first four EOFs of the observed zonal component of the wind stress anomalies are shown in Fig. 13. The first two EOFs are asymmetric about the equator. The first EOF explains only a small fraction of the total variance (15.7%) and each of the first three EOFs explain comparable fractions of the total variance. Thus, the observed stress has considerable variance for higher EOFs. The structures of the first two EOFs (Fig. 13a,b) agree well with those calculated by Latif et al. (1990). The variances explained by the first few EOFs in their study are much larger because they used observed wind stresses from which high frequencies (periods less than 16 months) were filtered. Figure 14 shows the first four EOFs of the zonal component of the surface wind stress τ^{x_m} produced by the atmospheric model during the control experiment. The first EOF here explains a large fraction of the total variance (84.6%). The other EOFs explain much smaller fractions of the total variance compared to the first EOF. In contrast to the structure of the observed surface winds, the structure of the first EOF of the model-produced surface winds is symmetric about the equator in the western Pacific. This inability of the atmospheric model to produce the correct structure of the first few EOFs (the asymmetries) is probably a serious problem in the coupled model.

This inability of the atmospheric model can be attributed to the nature of its response to the underlying SSTA, which was studied by Zebiak (1986). In the present case, the first four EOFs of the SSTA from the control experiment are shown in Fig. 15. The first EOF of the SSTA corresponds to the mature El Niño signal and explains 64.9% of the total variance. The first EOFs of the SSTA and that of the τ^{x_m} seem to explain relatively large fractions of the total variance of their respective fields. An illustration of the relationship between the first EOFs of the two fields is seen in Figs. 16a,b, where the time series of the amplitudes of the first two EOFs for SSTA and τ^{x_m} are shown. The time series of the amplitudes of the first two EOFs of the zonal component of the observed wind stress (τ^{x_o}) are shown in Fig. 16c. Note that the first EOF of the SSTA and that of τ^{x_m} have almost *identical* variations and that the second EOFs of both SSTA and τ^{x_m} have amplitudes much smaller that the first EOFs. These results suggest that the atmospheric model behaves like a

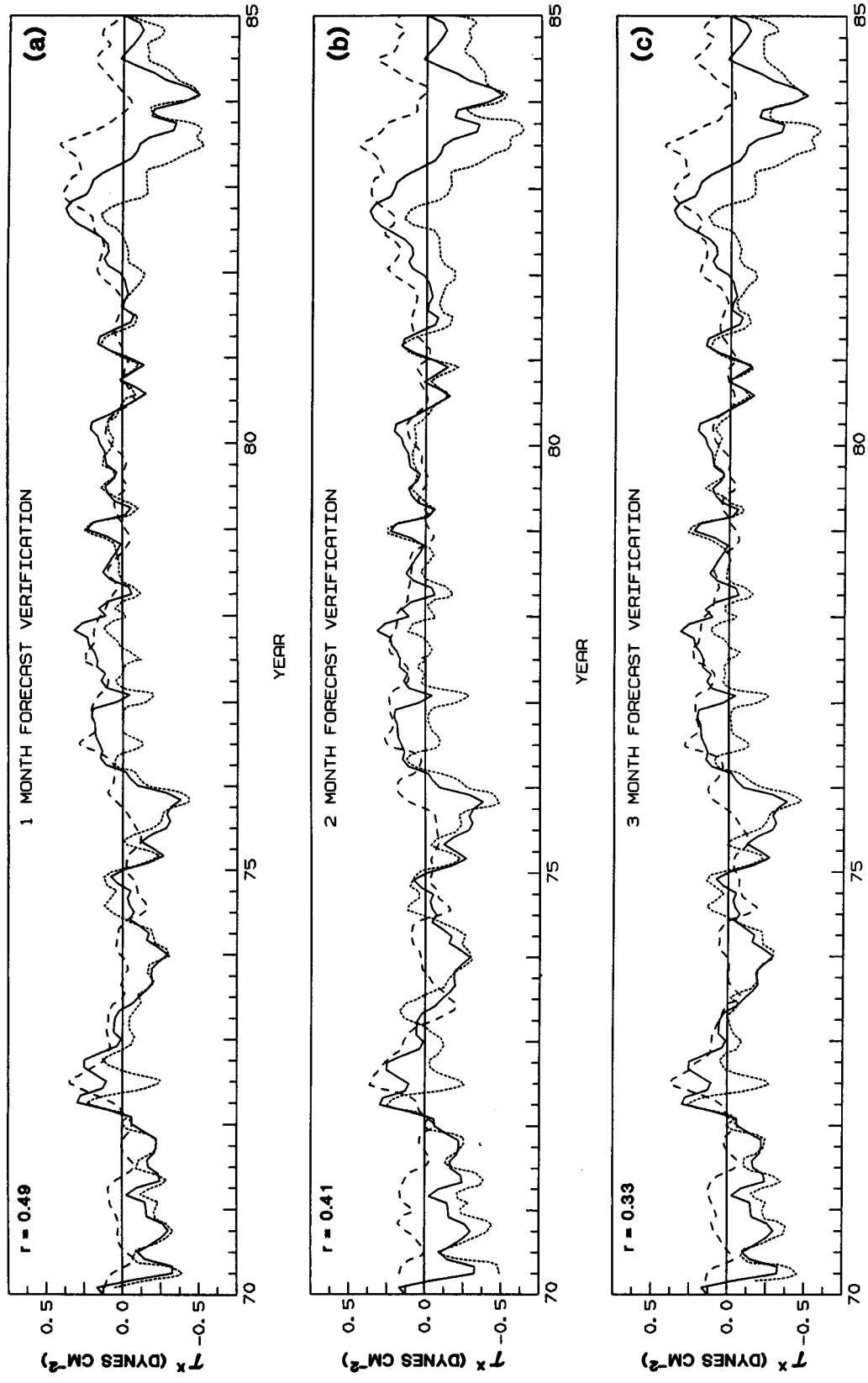

FIG. 11. Verification of forecasts for NINO4-averaged zonal component of the surface stress for all (a) one-month forecasts, (b) two-month forecasts, and (c) three-month forecasts. Solid = observed, Dashed = forecasts, Dotted = error (observed minus forecasts). The correlation (r) between the forecasts and the observations is also shown.

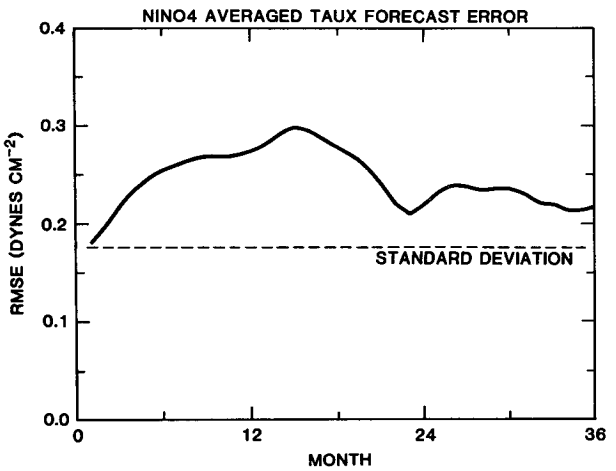

FIG. 12. Rms forecast error for the NINO4-averaged zonal component of the surface stress.

"slave" to the SST variations. This is not unexpected for this type of model, as suggested by Gill (1985). However, it is worth noting that the addition of a convergence feedback (Zebiak 1986) also does not seem to alter this character of the model's response significantly. This indicates that the coupled model simulates only one possible mode of variability. This point was also noted by Battisti and Hirst (1989).

It was noted earlier that the El Niño events simulated by the coupled model have certain structural differences with observed El Niño events (Cane and Zebiak 1987). For example, the model El Niño has large positive SST anomalies still remaining near the eastern boundary during the peak phase. Moreover, the model's large positive anomalies (say >1°C) do not extend westward of the date line. Because the atmospheric model is driven by the SST anomalies, the ocean model's inability to correctly simulate the structure of El Niños introduces errors in simulating the surface winds by the atmospheric component. In this manner, the ocean model also contributes to the growth of forecast errors.

Having noted that the observed surface wind stress has significant variance in the smaller spatial scales of motion, the question then arises as to which of these reproduce the basic character of the ENSO-type low frequency variability in the model and which scales of motion act like noise. To answer this question, several sensitivity experiments were conducted. In the first experiment, the ocean model was forced by the part of the observed surface stress that projects only on the first EOF of the observed surface stress. In the second experiment, the ocean model was forced by the part of the observed surface stress that projects on the first two EOFs. The third experiment was similar to the first and second, but with the part of the wind stress projected on the first three EOFs. The fourth experiment uses the part of the wind stress projected onto the fourth through tenth EOFs. The time evolution of the NINO3 SSTA from all four experiments is compared with the observed NINO3 SSTA in Fig. 17. The RMS error and the correlation coefficients between the observed and simulated NINO3 SSTA are also shown in Fig. 17. It is noted that the rms error decreases and the correlation increases as the second and the third EOFs are retained in the wind stress. It is rather interesting that, with only the first three EOFs, the simulated SST anomalies agree better with observations (rms error = 0.62°C, correlation = 0.73) than the control (rms

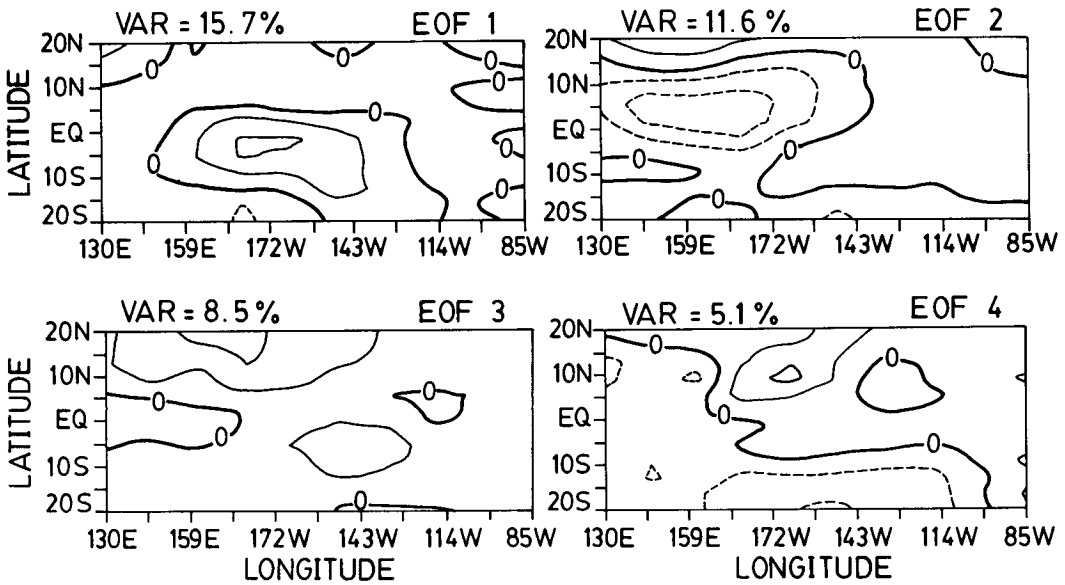

FIG. 13. The first four EOFs of the observed zonal component of the stress. Percentage of the total variance explained by each EOF is shown. Contour interval is 0.25 (arbitrary units).

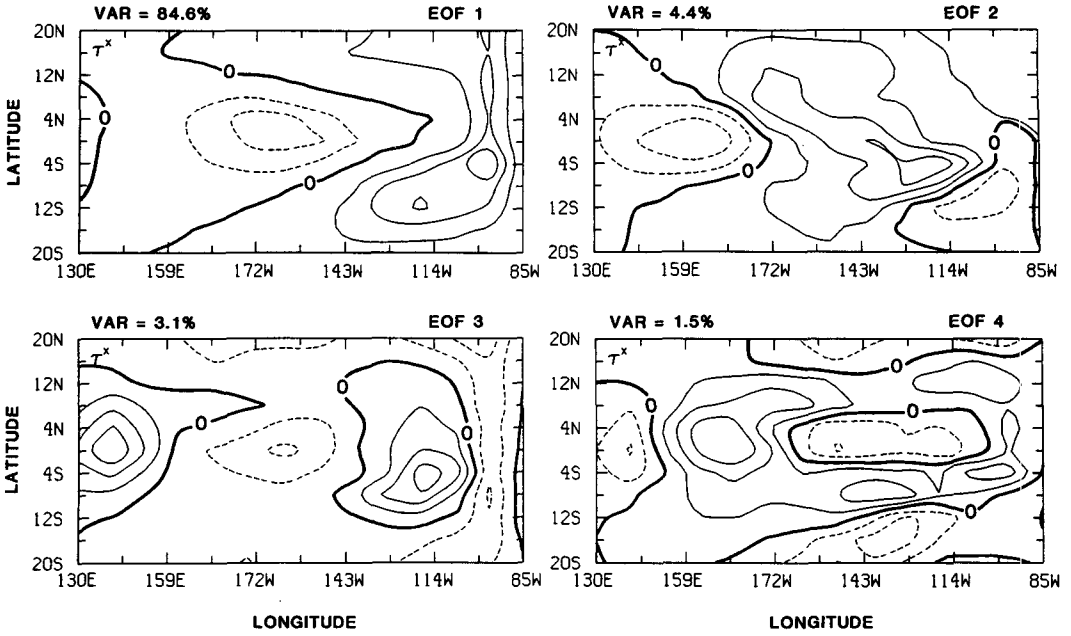

FIG. 14. The first four EOFs of the zonal component of the surface wind (u_a) produced by the atmospheric model during the control experiment. Percentage of the total variance explained by each EOF is shown. Contour interval is 0.25 (arbitrary units).

error = 0.72°C, correlation = 0.64), for which the total wind stress forcing was retained. In another experiment, where the first four EOFs were used, the RMS error and the correlation between the simulated and observed NINO3 SSTA (not shown in Fig. 17) were found to be 0.62°C and 0.72, respectively. Thus, the addition of the fourth EOF to the first three EOFs does not improve the simulation. If one retained more and more modes with higher and higher horizontal structures, one would eventually reproduce the control (Fig. 1).

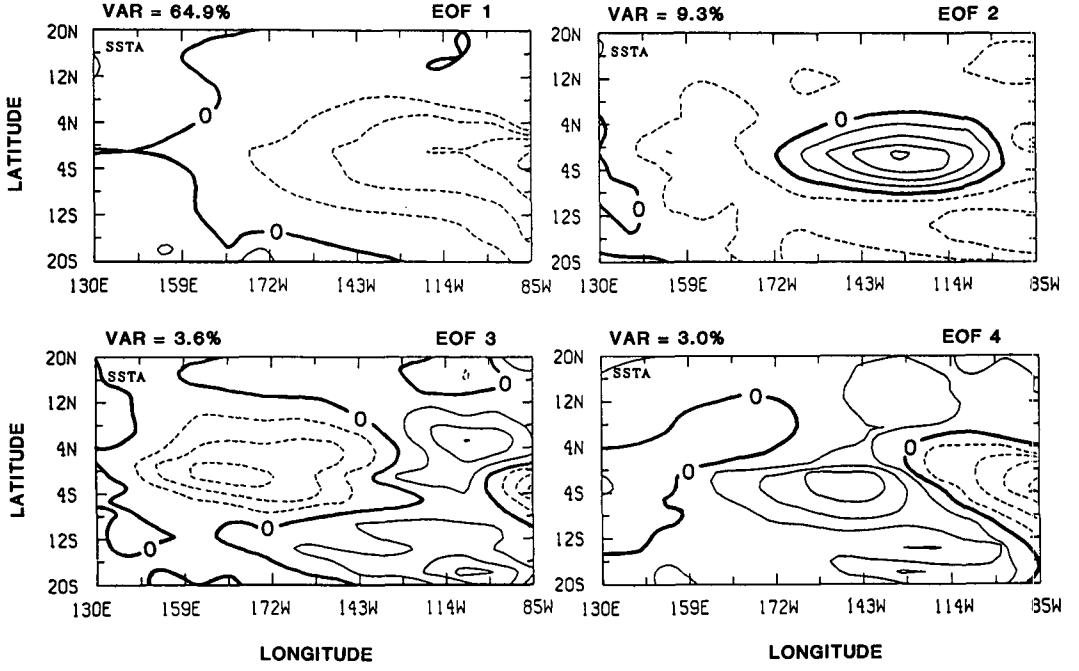

FIG. 15. The first four EOFs of the SSTA for the control experiment. Percentage of total variance explained by each EOF is shown. Contour interval is 0.25 (arbitrary units).

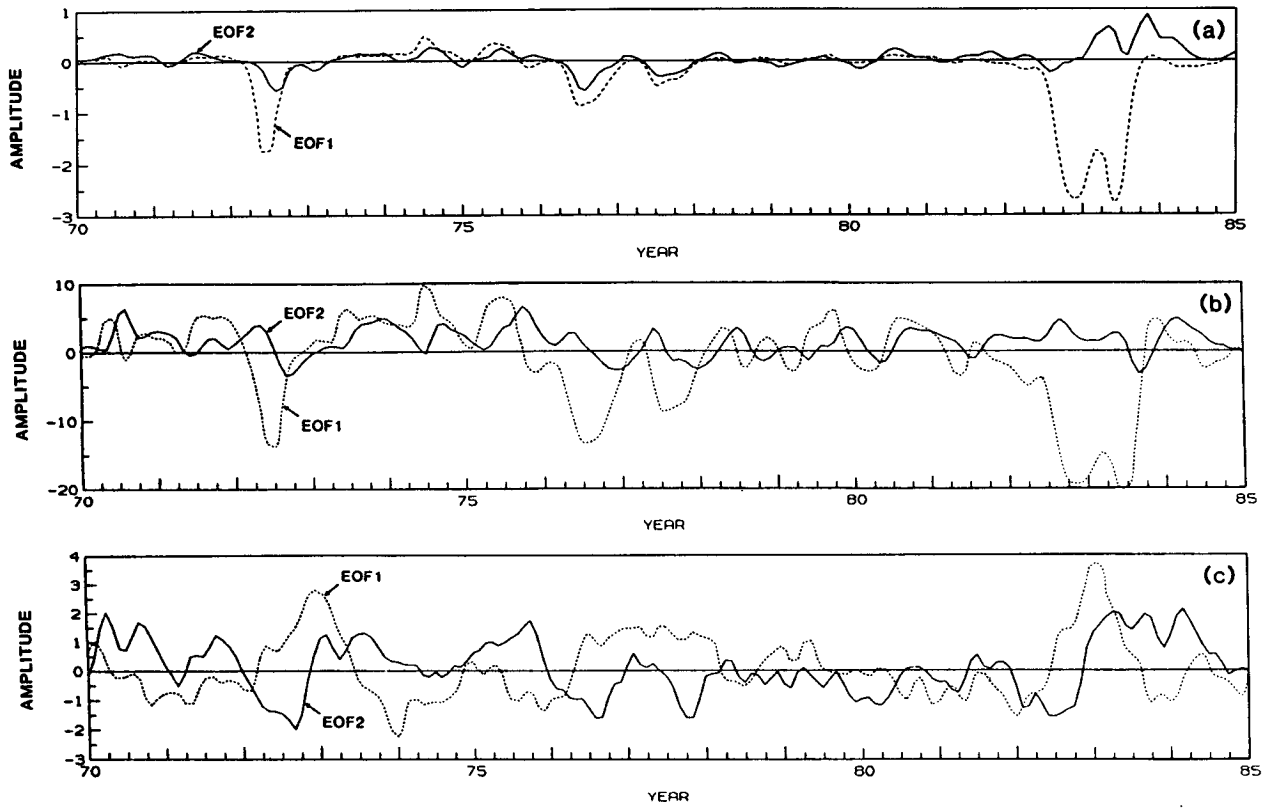

FIG. 16. Time series of the amplitude of the first two EOFs. (a) EOFs of the zonal wind from the atmospheric model (dyn cm^2). (b) EOFs of the SSTA from the control experiment (°C); and (c) EOFs of the zonal component of the observed stress (dyn cm^2).

Therefore, for the dominant interannual variations in the tropical Pacific, only the three largest scales of motion in the wind stress variability are needed. In a recent study, Latif et al. (1990) arrived at a similar conclusion by forcing their complex ocean GCM by the first two EOFs of the observed wind stress forcing. The modes with small horizontal scales in the wind stress essentially act like noise. This is also clear from Fig. 17d. If the first three modes are removed from the forcing, the remaining part of the wind stress cannot simulate the observed interannual variations.

If only the first EOF of the wind stress anomalies is retained, significant errors occur during the initiation phase of the warm events (Fig. 17a). The mature phases of the warm events are, however, well simulated. The westerly anomalies over the central Pacific associated with the first EOF of the observed wind stress anomalies (Fig. 13a) thus appear to be mainly connected with the response of the atmosphere due to the SSTA associated with the mature phase of the warm events. On the other hand, the initiation phase of the warm events is best simulated if the second and third EOFs of the observed stress are retained in the wind stress forcing. This suggests that the westerly wind anomalies in the south equatorial western Pacific associated with the second and third EOFs of the observed stress could be important in initiating the model-simulated warm events.

6. Summary and conclusions

In this study, an attempt has been made to determine the limits on the predictability of the coupled ocean–atmosphere system. This has been done by using the coupled model of Zebiak and Cane and following the classical methods developed for atmospheric predictability studies. This model is one of the simplest that reproduces realistically many of the important features of the observed interannual variability of SST in the tropical Pacific Ocean when forced by observed wind stresses.

To obtain an average measure for the growth of small initial errors, a large ensemble of prediction experiments was carried out. Because no reasonable analysis is available for all the fields, initial conditions for these prediction experiments were from a model control run in which the ocean model was forced by the observed surface winds. A detailed examination of the prediction errors was done making comparisons with the control simulation. This has shown that errors become larger than those of persistence or the long term standard deviation of the control by about three months. It

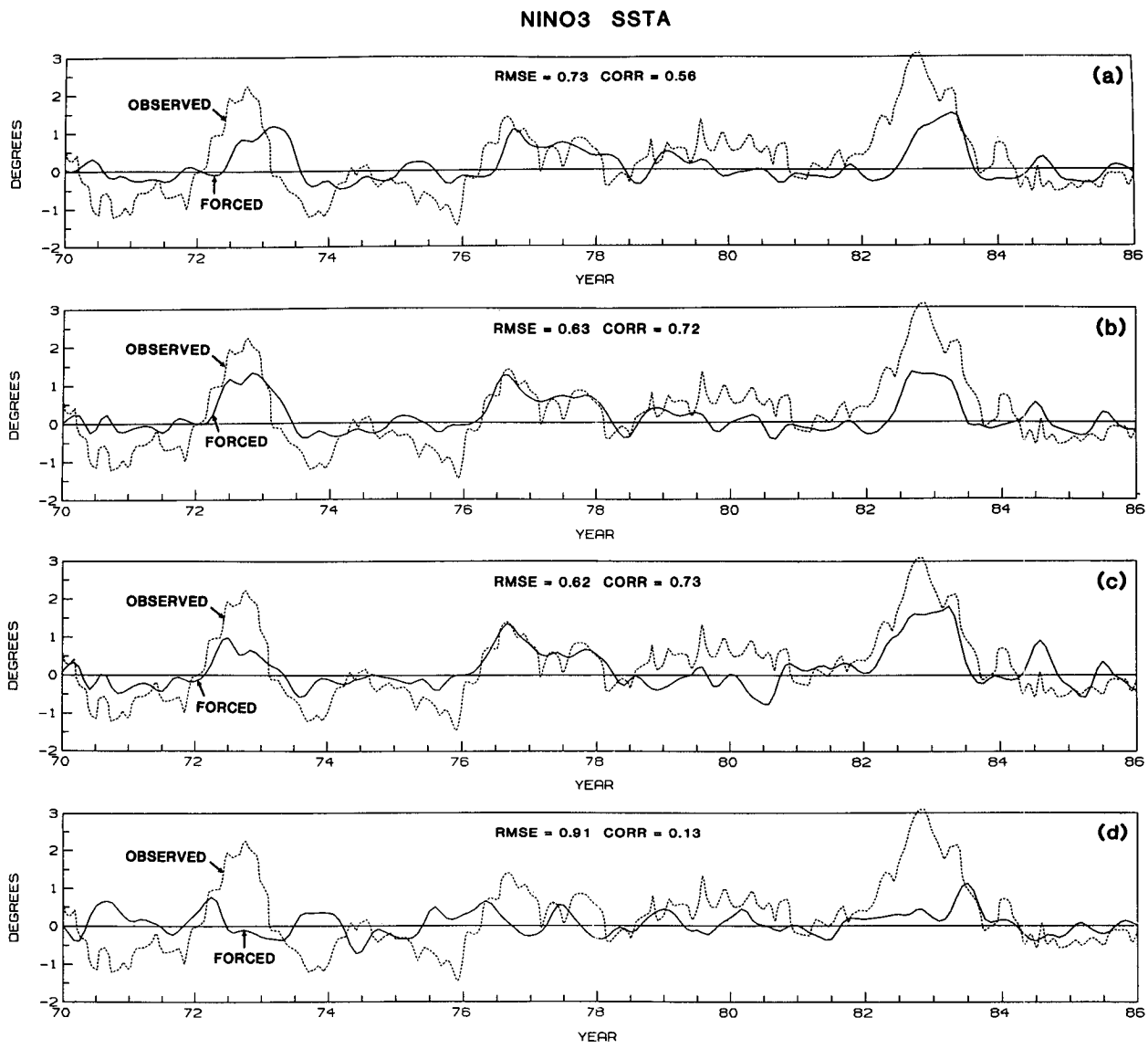

FIG. 17. Time series of the observed NINO3 SSTA (dotted curve) and those from the forced experiments (solid curve). (a) Forced only by EOF-1 of the observed stress; (b) forced by EOF-1 and EOF-2 of the observed stress; (c) forced by EOF-1, EOF-2, and EOF-3 of the observed stress; and (d) forced by EOFs 4–10 of the observed stress. The Rms error and the correlation between the observed SSTA and that from the truncated stress experiment are also shown.

should be emphasized, however, that this only gives a very gross measure of the growth of errors in the coupled model. For the prediction of special events such as the ENSO, this may not be the correct measure for prediction skill. In agreement with studies by Cane et al. (1986), Cane and Zebiak (1987, 1988), and Barnett et al. (1987), it was found that the predictions starting in the boreal winter have better skill than those starting in spring or summer.

Predictability studies have shown that the growth of small errors in the coupled model is governed by processes with two different time scales. The faster time scale process has an error doubling time of about 5 months, while the slower time scale has a doubling time of about 15 months. The fast time scale process tends to saturate the error at a level comparable to the natural variability of the control. As a result, it tends to put an upper limit on the predictability of the system. The existence of the slow growing process gives some reason to believe that, theoretically, the system may have long-range predictability. However, the key to this success will depend on the ability to identify initial conditions that are insensitive to the faster growing process. It is proposed that the fast error growth results from the coupled instability in the ZC model, while the slow error growth is associated with the low fre-

quency ENSO mode of the system. This is consistent with recent results (Battisti 1988, 1989b; Battisti and Hirst 1989) related to the physics of the low frequency variability of the ZC model.

Diagnosis of the atmospheric model response shows that it behaves like a *slave* to the SST anomalies. An EOF analysis of the surface wind stress produced by the atmospheric model shows that the first EOF explains 84.6% of the total variance, while the second EOF explains 4.4% of the total variance. The smaller scales explain a small fraction of the total variance. On the other hand, the first EOF of the observed wind stress anomalies explains only 15.7% of the total variance. The second and the third EOFs of the observed wind stress anomalies explain 11.6% and 8.5%, respectively. Thus, the first three EOFs of the observed wind stress together explain only 35.8% of the total variance. A large fraction of the total variance of the observed wind stress is therefore contained in the smaller spatial scales. Moreover, the structure of the largest two EOFs of the model-produced stress is symmetric about the equator, while that of the largest two EOFs of the observed stress is asymmetric about the equator. This means that the model is not able to produce the major wind anomalies at and near the equator correctly. This is probably a major problem with this model.

Although the observed surface wind stress has considerable signal in the smaller spatial scales of motion, it is not clear whether the component of the atmospheric forcing at these scales is important for simulating the interannual signal under consideration. Our sensitivity studies have shown that only a few spatial components of the observed surface wind forcing are required to simulate interannual variations. The small-scale components seem to act as noise and degrade the simulation when retained in the wind forcing. This apparent lack of impact of the small spatial components of wind forcing on simulating interannual variations in the tropics is thought to be an important finding and increases the hope of enhanced predictability of the coupled system. Even though most of the variance of the surface winds produced by the model is contained only in the first few EOFs, the model will do better if the structure of these EOFs agrees well with those of the observed surface wind stress.

It has been shown that the atmospheric component of the coupled model introduces large errors in the surface winds within one month of the predictions. As a result, the one-month prediction errors introduced by the coupled model are already large. These errors then grow following the instabilities of the coupled system. The average one-month prediction error in the SSTA is on the order of 0.2°C (Fig. 5a). If the model did not introduce additional errors, this initial error would grow to be as large as the natural variability of the control run (SD $\approx$ 0.71°C) in about 12 months. However, the prediction errors in the coupled model become as large as the SD in just three months. This indicates that the model is introducing additional errors during subsequent months of the prediction as well. Certainly, the atmospheric model is responsible for a part of the one-month prediction error. It appears that the atmospheric model is also partly responsible for the additional error during later months of the prediction as it continues to produce errors in the forcing field. Thus, as the atmospheric model is improved, it will not only reduce the one-month prediction errors but will also reduce additional errors during the subsequent months of the predictions. Also noted was that a part of the error in the surface wind predictions arises due to the tight coupling of the atmosphere to the SST anomalies and the ocean model's inability to simulate correct SST anomalies.

Finally, the following comment is offered on a direction in which improvements of the coupled model might proceed. Surely, the atmospheric component of the model needs improvement. At this point, however, it is not believed that coupling the oceanic model to an atmospheric general circulation model (AGCM) will solve the problem entirely unless systematic errors of AGCMs are significantly reduced. Limitations of atmospheric models will put a limit on the predictability of the low-frequency fluctuations of the ocean. However, for the first time it has been shown that only a few low-frequency components of the surface wind stress are required to simulate low frequency oceanic variability. This suggests that if an atmospheric model can be developed that is successful in simulating just this part of the wind stress variability, the coupled model may be more successful.

Acknowledgments. The authors sincerely thank Drs. Mark Cane and Steve Zebiak of Lamont Doherty Laboratory for graciously supplying us with the code for their model and wind forcing datasets. We have also benefited profoundly by several stimulating discussions with them and Dr. E. Sarachik. We thank Dr. David Battisti and Dr. Mojib Latif for their comments on an earlier draft of the manuscript. We would like to thank Ms. Marlene Schlichtig for typing the manuscript and Ms. Laura Rumburg for drafting the figures. This research was supported by NSF ATM-87-13567 and NASA NAGW-558.

REFERENCES

Anderson, D. L. T., and J. P. McCreary, 1985: Slowly propagating disturbances in a coupled ocean atmosphere model. *J. Atmos. Sci.*, **42**, 615–629.

Barnett, T. P., 1983: Interactions of the monsoon and the Pacific trade wind system at interannual time scales. Part I: The equatorial zone. *Mon. Wea. Rev.*, **111**, 756–773.

——, 1984: Prediction of the El Niño of 1982–83. *Mon. Wea. Rev.*, **112**, 1403–1407.

——, N. Graham, M. Cane, S. Zebiak, S. Dolan, J. O'Brien and D. Legler, 1988: On the prediction of the El Niño of 1986–87. *Science*, **241**, 192–196.

Battisti, D. S., 1988: Dynamics and thermodynamics of a warming

event in a coupled tropical atmosphere–ocean model. *J. Atmos. Sci.*, **45**, 2889–2919.

——, 1989a: On the role of subtropical oceanic Rossby waves during ENSO. *J. Phys. Oceanogr.*, **19**, 551–559.

——, 1989b: Interannual variability in coupled tropical atmosphere–ocean models. *Climate and Ocean Dynamics.* M. E. Schlesinger, Ed., Kluwer Academic Publishers.

——, and A. C. Hirst, 1989: Interannual variability in the tropical atmosphere–ocean system: influence of the basic state and ocean geometry. *J. Atmos. Sci.*, **46**, 1687–1712.

——, —— and E. S. Sarachik, 1989: Instability and predictability in coupled atmosphere–ocean models. *Phil. Trans. Roy. Soc. London*, A**329**, 237–247.

Bigg, G. R., and J. R. Blundell, 1989: The equatorial Pacific Ocean prior to and during El Niño of 1982–83—a normal mode model view. *Quart. J. Roy. Meteor. Soc.*, **115**, 1039–1069.

Busalacchi, A. J., and J. J. O'Brien, 1981: Interannual variability of the equatorial Pacific in the 1960s. *J. Geophys. Res.*, **86**, 10 901–10 907.

Cane, M. A., and S. E. Zebiak, 1987: Prediction of El Niño events using a coupled model. *Atmospheric and Oceanic Variability.* H. Cattle, Ed., Royal Meteorological Society, 153–181.

——, and ——, 1988: Dynamical forecasts of the 1986-87 ENSO with a coupled model. *Proc. of the 13th Annual Climate Diagnostics Workshop*, NOAA, pp. 278–282.

——, —— and S. C. Dolan, 1986: Experimental forecasts of El Niño. *Nature*, **321**, 827–832.

Carton, J. A., and J. Shukla, 1990: Predictability of the tropical Atlantic Ocean. *J. Mar. Sys.*, **15**,

Charney, J. G., and J. Shukla, 1981: Predictability of monsoons. *Monsoon Dynamics.* Sir James Lighthill and R. P. Pearce, Eds., Cambridge University Press, 99–110.

——, R. G. Fleagle, H. Riehl, V. E. Lally and D. Q. Wark, 1966: The feasibility of a global observation and analysis experiment. *Bull. Amer. Meteor. Soc.*, **47**, 200–220.

Dalcher, A., and E. Kalnay, 1987: Error growth and predictability in operational ECMWF forecasts. *Tellus*, **39A**, 474–491.

Fennessy, M. J., L. Marx and J. Shukla, 1985: GCM sensitivity to 1982–83 equatorial Pacific temperature anomalies. *Coupled Ocean Atmosphere Models.* J. C. J. Nihoul., Ed., Elsevier Publishers, 121–130.

Fraedrich, K., 1988: El Niño–Southern Oscillation predictability. *Mon. Wea. Rev.*, **116**, 1001–1012.

Gill, A. E., 1985: Elements of coupled ocean–atmosphere models for the tropics. *Coupled Ocean Atmosphere Models.* J. C. J. Nihoul, Ed., Elsevier Publisher, 303–328.

Goldenberg, S. O., and J. J. O'Brien, 1981: Time and space variability of tropical Pacific wind stress. *Mon. Wea. Rev.*, **109**, 1190–1207.

Graham, N. E., J. Michaelsen and T. P. Barnett, 1987: An investigation of the El Niño–Southern Oscillation cycle with statistical models. Part I: Predictor field characteristics. *J. Geophys. Res.*, **92C**, 14 251–14 270.

Hirst, A. C., 1986: Unstable and damped equatorial modes in simple coupled ocean–atmosphere models. *J. Atmos. Sci.*, **43**, 606–630.

——, 1988: Slow instabilities in tropical ocean basin–global atmosphere models. *J. Atmos. Sci.*, **45**, 830–852.

Hoffman, R., and E. Kalnay, 1983: Lagged averaged forecasting; an alternative to Monte Carlo forecasting. *Tellus*, **35A**, 100–118.

Inoue, M., and J. J. O'Brien, 1984: A forecasting model for the onset of a major El Niño. *Mon. Wea. Rev.*, **112**, 2326–2337.

Latif, M., 1987: Tropical ocean circulation experiments. *J. Phys. Oceanogr.*, **17**, 246–263.

——, J. Biercamp, H. V. Storch, M. McPhaden and E. Kirk, 1990: Simulation of ENSO-related surface wind anomalies with an atmospheric GCM forced by observed SST. *J. Climate*, **3**, 509–521.

Lau, N. C., 1985: Modeling the seasonal dependence of the atmospheric response to observed El Niños 1962–1976. *Mon. Wea. Rev.*, **113**, 1970–1996.

Lorenz, E. N., 1963: The predictability of hydrodynamic flow. *Trans. New York Acad. Sci.*, **25**, 409–432.

——, 1965: A study of the predictability of a 28-variable atmospheric model. *Tellus*, **17**, 321–333.

——, 1982: Atmospheric predictability experiments with a large numerical model. *Tellus*, **34**, 505–513.

Miyakoda, K., C. T. Gordon, R. Caverly, W. F. Stern, J. Sirutis and W. Bourke, 1983: Simulation of a blocking event in January, 1977. *Mon. Wea. Rev.*, **111**, 846–869.

Philander, S. G. H., and A. D. Seigel, 1985: Simulation of El Niño of 1982–1983. *Coupled Ocean-Atmosphere Models.* J. C. J. Nihoul, Ed., Elsevier, 517–541.

——, and N. C. Lau, 1988: Predictability of El Niño. *Physically Based Modeling and Simulation of Climate and Climate-Change. Part II.* M. E. Schlesinger, Ed., Kluwer Academic Publishers, 967–982.

——, T. Yamagata and R. C. Pacanowski, 1984: Unstable air–sea interactions in the tropics. *J. Atmos. Sci.*, **41**, 604–613.

Reynolds, R. W., 1988: A real-time global sea surface temperature analysis. *J. Climate*, **1**, 75–86.

Schopf, P. S., and M. J. Suarez, 1988: Vacillations in a coupled ocean–atmosphere model. *J. Atmos. Sci.*, **45**, 549–566.

Seager, R., 1989: Modeling tropical Pacific sea surface temperature: 1970–87. *J. Phys. Oceanogr.*, **19**, 419–434.

——, S. E. Zebiak and M. A. Cane, 1988: A model of tropical Pacific sea surface temperature climatology. *J. Geophys. Res.*, **93C**, 1265–1280.

Shukla, J., 1981: Dynamical predictability of monthly means. *J. Atmos. Sci.*, **38**, 2547–2572.

——, 1985: Predictability. *Advances in Geophysics*, Vol. 28B, Academic Press, 87–122.

Smagorinsky, J., 1969: Problems and promises of deterministic extended range forecasting. *Bull. Amer. Meteor. Soc.*, **50**, 286–311.

Yamagata, T., 1985: Stability of a simple air–sea coupled model in the tropics. *Coupled Ocean–Atmosphere Models.* J. C. J. Nihoul, Ed., Elsevier, 637–658.

Zebiak, S. E., 1986: Atmospheric convergence feedback in a simple model for El Niño. *Mon. Wea. Rev.*, **114**, 1263–1271.

——, 1989: Oceanic heat content variability and El Niño cycles. *J. Phys. Oceanogr.*, **19**, 475–486.

——, and M. A. Cane, 1987: A model El Niño–Southern Oscillation. *Mon. Wea. Rev.*, **115**, 2262–2273.